Talanta 124 (2014) 27–35

Contents lists available at ScienceDirect

Talanta

journal homepage: www.elsevier.com/locate/talanta

Fabrication of an ultrasensitive impedimetric buprenorphine hydrochloride biosensor from computational and experimental angles

Mohammad-Bagher Gholivand [a,*], Ali R. Jalalvand [a,b], Hector C. Goicoechea [b], Thomas Skov [c]

[a] Faculty of Chemistry, Razi University, Kermanshah 671496734, Iran
[b] Laboratorio de Desarrollo Analítico y Quimiometría (LADAQ), Cátedra de Química Analítica I, Universidad Nacional del Litoral, Ciudad Universitaria, CC 242 (S3000ZAA), Santa Fe, Argentina
[c] Quality & Technology, Department of Food Science, Faculty of Science, University of Copenhagen, Copenhagen, Denmark

ARTICLE INFO

Article history:
Received 24 November 2013
Received in revised form
5 February 2014
Accepted 7 February 2014
Available online 18 February 2014

Keywords:
Biosensor
Buprenorphine hydrochloride
Bovine serum albumin
Multi-walled carbon nanotubes
Computational and experimental characterizations

ABSTRACT

For the first time, an ultrasensitive impedimetric buprenorphine hydrochloride (BN) biosensor based on immobilization of bovine serum albumin (BSA) onto multi-walled carbon nanotubes (MWCNTs)/glassy carbon electrode (BSA/MWCNTs/GCE) has been developed using initial characterization by computational methods and complementing them by experimental observations. Computational results showed that the BSA hydrophobically binds to MWCNTs which is energetically favorable and leads to spontaneous formation of the stable BSA/MWCNTs nanobiocomposite (bioconjugate). Computational results also showed that the interaction of BN with BSA is mainly driven by hydrophobic interactions. The interactions of BSA with MWCNTs and BN with BSA were also monitored by fluorescence and UV–vis spectroscopic techniques, and their results were consistent with the computational results. Morphology and electrochemical properties of the fabricated composite electrodes were examined by scanning electron microscopy (SEM), cyclic voltammetry (CV), and electrochemical impedance spectroscopy (EIS). Besides complementing the computational studies, experimental results showed that the addition of MWCNTs to the surface of the GCE greatly facilitated the electron transfer reactions, and also showed that the presence of BSA inhibits the interfacial electron transfer in some extent due to the non-conductive properties of BSA. On the other hand, the presence of BN may form an electroactive complex with BSA which accelerates the interfacial electron transfer and leads to obvious Faradaic impedance changes. The Faradaic impedance responses were linearly related to BN concentration between 5.0 nM and 72.0 nM and a limit of detection (LOD, $3S_b/b$) of 1.5 nM was achieved. Finally, the proposed biosensor was successfully applied to determination of BN in urine samples of both healthy and addict volunteers. The results were satisfactory and comparable to those obtained by applying the reference method based on high performance liquid chromatography-ultraviolet detection (HPLC-UV). It is expected that the distinctive features of BSA/MWCNTs nanobiocomposite would make it potentially advantageous for a broad range of biosensing, and clinical applications.

1. Introduction

Buprenorphine (BN, Fig. 1A) is a strong semi-synthetic opiate painkiller with a sovereignty of 20–40 times higher than that of morphine [1]. It is commonly used at higher doses for treating opioid addiction and at lower doses for controlling both moderate to acute pains in non-opioid-tolerant individuals and moderate chronic pains [1]. BN causes three major effects of diminished respiration, gladness, and reduced pain. In fact, at high doses and under certain circumstances, BN not only blocks the effects of full opioid agonists but also precipitates withdrawal symptoms [2]. As an analgesic, it has been successfully used via intramuscular,

Abbreviations: BSA, bovine serum albumin; HSA, human serum albumin; BN, buprenorphine hydrochloride; MWCNTs, multi-walled carbon nanotubes; GCE, glassy carbon electrode; SEM, scanning electron microscopy; CV, cyclic voltammetry; EIS, electrochemical impedance spectroscopy; LOD, limit of detection; UPW, ultrapure water; SCE, saturated calomel electrode; MVD, molegro virtual docker; PBS, phosphate buffered solution; RSD, relative standard deviation; HPLC-UV, high performance liquid chromatography-ultraviolet; DMF, dimethylformamide

* Corresponding author. Tel.: +98 831 4274557; fax: +98 831 4274559.
E-mail addresses: mbgholivand2013@gmail.com, mbgholivand@yahoo.com (M.-B. Gholivand).

http://dx.doi.org/10.1016/j.talanta.2014.02.017
0039-9140

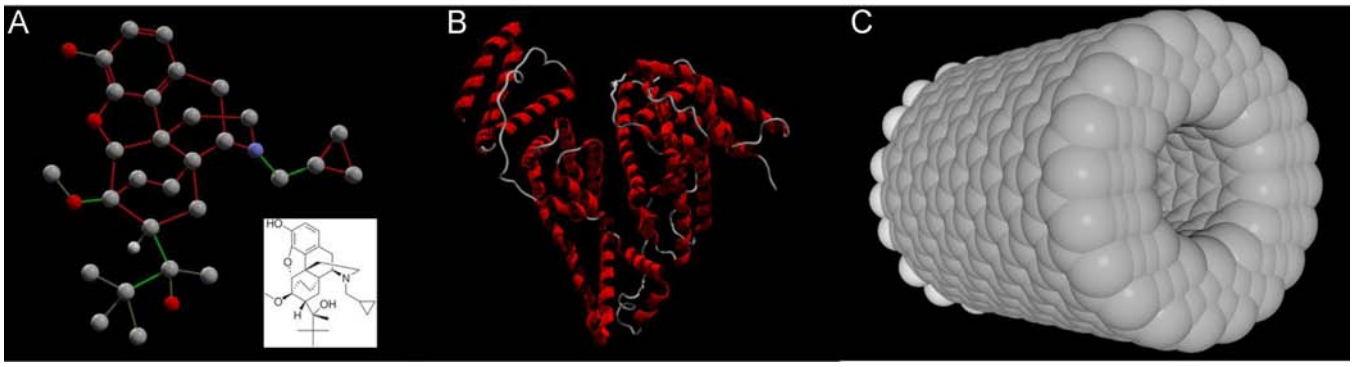

Fig. 1. (A) Molecular structure of BN represented by the ball and stick model, (B) three-dimensional structure of BSA (chain A) represented by solid ribbons, and (C) structure of the MWCNTs designed by Nanotube Modeler software and represented by the CPK model.

intravenous, or sublingual paths for appeasing moderate to severe and chronic pains [3]. Like other opiates, it has been reportedly abused [4] as in the doping of racehorses [5]. Therefore, the matrices in which BN could be defined are very different, especially in biological samples.

Different methods have been reported for the determination of BN, including adsorptive stripping voltammetry [6], gas chromatography–mass spectrometry [7–10], radioimmunoassay [5], and high performance liquid chromatography (HPLC) [11–17]. As a powerful technique for the determination of pharmaceutical compounds in biological fluids, electrochemical techniques can be considered as a suitable and sensitive alternative to other instrumental methods [18–22]. Among the electrochemical methods, electrochemical impedance spectroscopy (EIS) technique becomes increasingly popular because it offers several advantages such as simplicity, high sensitivity and serving as an elegant way to interface biorecognition events and signal transduction.

Among biomacromolecules, serum albumin is a soluble protein, which is a major constituent of the circulatory system, and it commonly serves as a depository and a transport molecule for many exogenous compounds. Bovine serum albumin (BSA, Fig. 1B) is one of the most extensively studied of this group of proteins, particularly because of its structural homology with human serum albumin (HSA). The direct electron transfer between proteins and the electrode surface has received considerable attention, because it can be used in fabricating new generation of biosensor devices. Since redox centers are deeply buried within the protein molecules, the electron transfer between proteins and the electrode is difficult. Therefore, many efforts have been devoted to immobilizing proteins on the electrode surface modified with various films. With good conductance, electrocatalytic properties and chemical stability, carbon nanotubes (CNTs) have been investigated extensively [23–25].

The objective of this study is to develop a novel, ultrasensitive, selective and simple impedimetric BN biosensor with good stability, reproducibility and repeatability for determination of BN using unique properties of BSA/MWCNTs nanobiocomposite (bioconjugate) which can be directly applied in urine samples without expensive and time-consuming pretreatments. To demonstrate the general design of the BSA/MWCNTs nanocomposite based biosensing platform, we first used computational studies for a proof of concept and then completed them by experimental observations. This valuable study describes the results obtained by a combination of computational and experimental techniques to develop an ultrasensitive BSA/MWCNTs/GCE biosensor for direct determination of BN in urine samples of both healthy and addict volunteers. To the best of our knowledge, there are only two works in the literature related to the determination of BN using electrochemical methods [6,26], and this work is the first report on the impedimetric BN biosensor.

2. Experimental

2.1. Chemicals and solutions

The BSA ($M=66487$, free of fatty acids with an electrophoresis grade), BN, and MWCNTs (purity > 95%) were purchased from Sigma-Aldrich (St. Louis, MO, USA). All other reagents employed were of analytical grade and received from Merck. A concentration of 0.067 M phosphate buffer solution (PBS, prepared from NaH_2PO_4 and Na_2HPO_4) was used to control the pH at 7.4. $[Fe(CN)_6]^{3-/4-}$ solution (redox probe, 5.0 mM) was prepared in PBS (0.067 M, pH 7.4) and used for the measurements. A stock standard solution of BN was prepared in methanol with a concentration level of 0.01 M, and was stored in a freezer at −20 °C. Working solutions were prepared by appropriate dilution of the stock standard solution. A blank urine sample (drug-free) was collected from a healthy volunteer and an actual urine sample was obtained from a Medical Diagnostic Laboratory in Kermanshah, Iran, and stored at −20 °C prior to use. All solutions were prepared by ultrapure water (UPW).

2.2. Instruments and softwares

Electrochemical experiments were performed using a μ-AutolabIII/FRA2 controlled by the Nova software (Version 1.8). A conventional three-electrode cell was used with a saturated calomel electrode (SCE) as a reference electrode, a Pt wire as a counter-electrode and a bare or modified GCE as a working electrode. The EIS measurements were performed in the redox probe solution and plotted in the form of complex plane diagrams (Nyquist plots). The SEM experiments were performed by a KYKY-EM 3200 scanning electron microscope. All fluorescence spectra were measured using a Cary Eclipse fluorescence spectrophotometer equipped with a water bath and a 1.0 cm quartz cell. The UV–vis spectra were measured using an Agilent 8453 UV–vis Diode-Array spectrophotometer controlled by the Agilent UV–vis ChemStation software. A JENWAY-3345 pH-meter equipped with a combined glass electrode was used for pH measurements. High performance liquid chromatography-ultraviolet detection (HPLC-UV) analyses reported in this study were carried out in a Medical Diagnostic Laboratory in Kermanshah, Iran whose instrument was an 1100 Series HPLC from Agilent Technologies (Wilmington, DE, USA) equipped with a binary pump, degasser, auto-sampler, solvent tray and multiple wavelength detector. The statistical analysis of the sequence of BSA (chain A) was performed using CLC Main Workbench software (Version 6.0). The three-dimensional structure

of nanotubes was generated using Nanotube Modeler software by defining a diameter of 1.1 nm, tube length = 18 nm, and the chirality parameters $n = 14$ and $m = 0$ (Fig. 1C). Nanotubes were then docked to the BSA using Molegro Virtual Docker (MVD) software. The chemical structure of the BN was constructed by Hyperchem package (Version 8.0), and energy minimization for BN was performed by the AM1 semi-empirical method with the Polak–Ribiere algorithm until the root mean square gradient of 0.01 kcal mol^{-1}. The MVD software was also employed to generate a docked conformation of BN with BSA. LIGPLOT [27], a program for automatically plotting protein–ligand interactions, was used for analyzing the interactions between BN and BSA. The recorded experimental data was smoothed, when necessary, and converted to matrices by means of several homemade MATLAB (Version 8.1) files. All computations were run on a DELL XPS laptop (L502X) with Intel Core i7-2630QM 2.0 GHz, 8 GB of RAM and Windows 7-64 as its operating system.

2.3. Preparation of the electrochemical biosensor

The bare GCE was polished carefully using zinc oxide and alumina mixture with the help of a silky pad. The polished electrode was washed with UPW and then dried with nitrogen. A small amount (40.0 μl) of suspension of MWCNTs (0.5 mg mL^{-1}) in dimethylformamide (DMF) was put on the surface of bare polished GCE. It was seen that the suspension covered total surface area of the GCE. The suspension was allowed to be desiccated by keeping the electrode in open at room temperature (25.0 ± 0.2 °C). Within about half an hour, the solvent evaporated off leaving a thin layer of MWCNTs on the electrode surface. The electrode so obtained is called MWCNTs/GCE.

The BSA/MWCNTs/GCE was prepared with the following procedure: a 6.0 μL of the BSA solution (0.35 mg mL^{-1} dissolved in PBS at pH 7.4) was dripped on the MWCNTs/GCE surface and dried by passing very slow rate of air for 10.0 min to form a stable gel-like film. In some cases the BSA/MWCNTs/GCE was transferred to a BN solution (50.0 nM) and incubated for 30.0 min. Then, the electrode was extensively rinsed and subjected to electrochemical measurements. The refreshment of the bare GCE surface was achieved by sonicating the modified electrode surface in 0.1 M hydrochloric acid for 5.0 min and then acetonitrile for 5.0 min. The electrode surface was dried and then sensed again with the same composition for further experiments.

2.4. Preparation of the real samples

The blank urine sample (drug-free) was collected from a healthy volunteer, which was not exposed to any drug for at least 6 months. The actual urine sample was collected from a person who was addicted to opium which was provided by a Medical Diagnostic Laboratory in Kermanshah, Iran. Urine samples were kept frozen at −20.0 °C before analysis. The frozen urine samples were thawed at room temperature and centrifuged for 10.0 min at 5000.0 rpm. White lipidic solid was sedimented in the bottom of the conical test tube. The supernatants were transferred into clean glass tube and filtrated through a 0.45 μm filter.

3. Results and discussion

3.1. Computational studies

In order to gain preliminary insights related to the interaction of BSA with MWCNTs at the molecular level, both the sequence

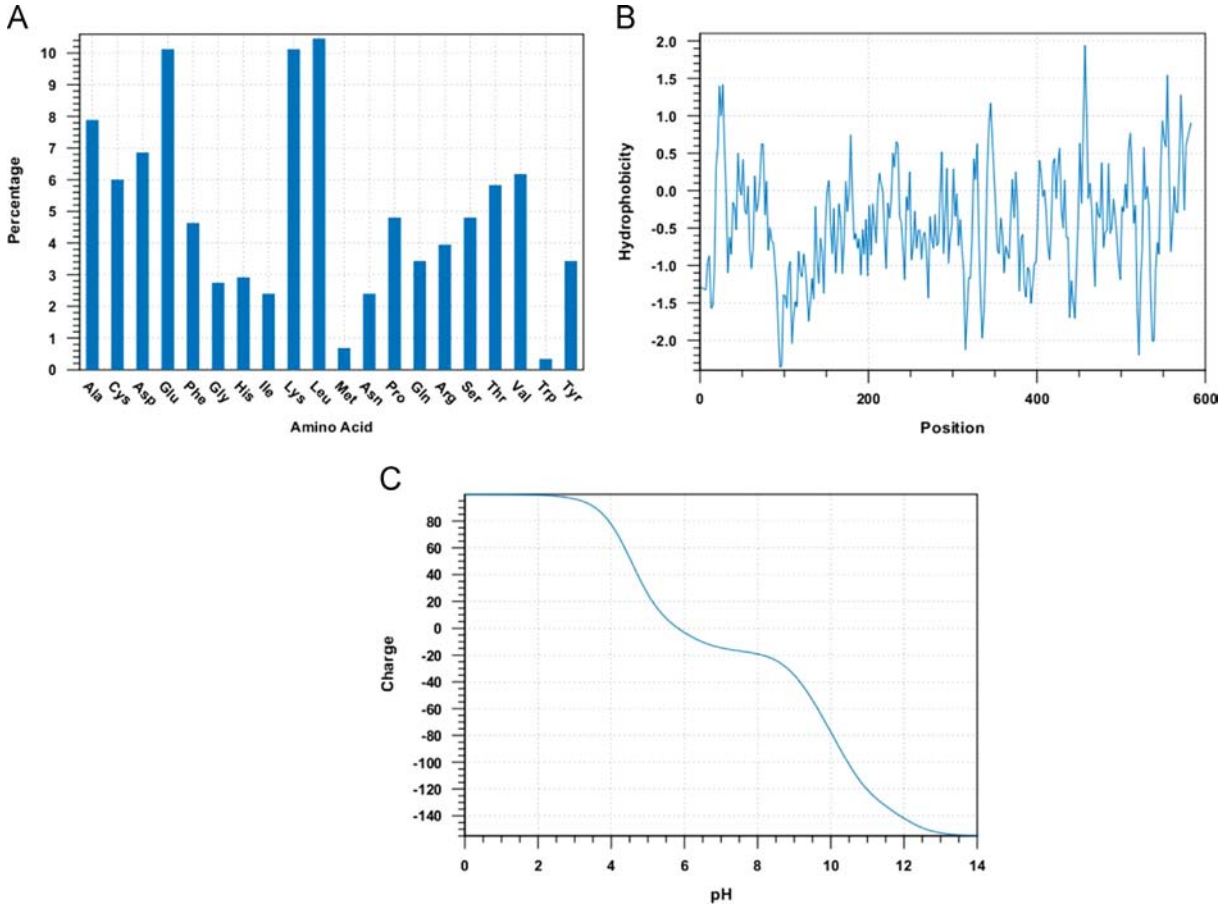

Fig. 2. Results of protein analysis: (A) amino acid distribution histogram, (B) hydrophobicity plot, and (C) electrical charge as a function of pH.

and the crystal structure of BSA (chain A) were investigated. The results pertinent to the sequence statistics showed that out of the 583 amino acids (Fig. 2A) composing the selected chain of BSA, approximately 40.1% were hydrophobic (A, F, G, I, L, M, P, V, and W) and 25.9% were hydrophilic (C, N, Q, S, T, and Y), Fig. 2B. More importantly, it was observed that the protein displays approximately the same number of negative and positive groups on its surface, and the calculated isoelectric point was approximately 5.2, Fig. 2C. Based on this information, it is reasonable to expect that the interaction of BSA with MWCNTs will be driven by a combination of hydrophobic and hydrophilic interactions, where the former prevails over the latter.

Subsequently, molecular docking studies were performed to identify the potential interaction sites, assuming that the MWCNTs (considered as ligand) would freely rotate around the entire structure of the BSA. Such docking studies enabled the identification of the most likely manner by which MWCNTs were bound to BSA. The docking results with three different views are shown in Fig. 3A–C. An additional advantage of the docking studies is the possibility to identify the BSA residues that interact the most with MWCNTs. As can be seen, MWCNTs are surrounded by Thr 83, Gln 33, Gly 85, Asp 86, His 105, Asp 107, Lys 465, Thr 466, Pro 420, Ser 418, Thr 419, Lys 533, Lys 499, and Glu 530. The docking of MWCNTs to BSA seems to be dominated by hydrophobic interactions. The binding constant (K_a) and free energy change (ΔG) for the binding of MWCNTs to BSA were $1.8\times10^5\ M^{-1}$ and $-14.58\ kJ\ M^{-1}$, respectively. Therefore, it is also reasonable to expect that the interaction of BSA with MWCNTs will be energetically favorable, leading to spontaneous formation of the nanobiocomposite. Hence, such interaction supports the possibility of using the BSA/MWCNTs nanobiocomposite with analytical purposes.

The MVD software was also used to realize the binding mode of BN at the BSA. The dockings results with three different views are shown in Fig. 4A–C. As can be seen, BN is surrounded by Tyr 160, Tyr 137, Phe 133, Lys 132, Lys 136, Leu 122, Glu 125, Pro 117, Thr 121, and Asp 118. The K_a and ΔG for the binding of BN to BSA were $2.3\times10^4\ M^{-1}$ and $-18.61\ kJ\ M^{-1}$, respectively. LIGPLOT was used to explore the types of interactions between BN and BSA as shown in Fig. 4D. Hydrogen bonding interaction was not observed between BN and BSA, but the results showed that the binding of BN to BSA was mainly driven by hydrophobic interactions. Based on this information, it is reasonable to expect that the interaction of the BN with BSA is mainly driven by hydrophobic interactions.

3.2. Experimental studies

3.2.1. Summarized fluorescence quenching and UV–vis absorption studies

3.2.1.1. Fluorescence quenching studies. In order to examine the interaction of MWCNTs with BSA, the fluorescence spectra were recorded in the PBS (0.067 M, pH 7.4) at three different temperatures including 298.15, 304.15, and 310.15 K and representative spectra at 298.15 are shown in Fig. 5A. A gradual increase of the MWCNTs concentration in the solutions of BSA resulted in a decrease of fluorescence intensity without notable changes in the wavelength of maximum emission. In order to further investigate the quenching form of BSA, the well-known Stern–Volmer equation (Eq. 1) was used to analyze the quenching data

$$F_0/F = 1 + k_q\tau_0[Q] = 1 + K_{SV}[Q] \quad (1)$$

where F_0 and F represent the fluorescence intensities in the absence and in the presence of quencher (MWCNTs), k_q is the quenching rate constant of the biomolecule, K_{SV} is the dynamic quenching constant, τ_0 is the average lifetime of the molecule without quencher, 10^{-8}, and $[Q]$ is the concentration of the quencher [28]. F_0/F versus $[Q]$ was plotted at 298.15, 304.15, and 310.15 K (not shown). K_{SV}, calculated by linear regression of the plots, are 0.0796, 0.0652, and 0.0531 M^{-1}, correspondingly, decreasing with temperature. Therefore, we concluded that this quenching process is static quenching.

Results from fluorescence measurements can be used to estimate the binding constant of the BSA–MWCNTs hybrid complex by a different form of the Stern–Volmer equation [29]:

$$\log\left(\frac{F_0-F}{F}\right) = \log K_a + n\log[Q] \quad (2)$$

where F_0, F, and $[Q]$ are the same as in Eq. 1, n is the number of average binding sites, and K_a is the binding constant. A plot of $\log[(F_0-F)/F]$ versus $\log[Q]$ yields $\log K_a$ as the intercept and n as the slope. The K_a and n values obtained at 298.15, 304.15, and 310.15 K are shown in Table 1. Values of n are approximately equal to 2, which indicate the existence of two binding sites in BSA for MWCNTs; the estimated values of K_a indicated that there is a moderately strong attraction between MWCNTs and BSA.

Generally speaking, the interaction forces between ligands and proteins include hydrogen bonds, van der Waals forces, electrostatic forces, and hydrophobic interaction forces [28]. From the thermodynamics point of view, $\Delta H>0$ and $\Delta S>0$ imply that a hydrophobic interaction is the main force; $\Delta H<0$ and $\Delta S<0$ reflect van der Waals forces or hydrogen bonding; $\Delta H<0$ and $\Delta S>0$ suggest that electrostatic forces play a key role [30]. When there is no significant change in temperature, the enthalpy of the reaction can be considered as a constant in the formulas by which we calculated the thermodynamic parameters:

$$\ln K = -\frac{\Delta H}{RT} + \frac{\Delta S}{R} \quad (3)$$

where ΔH, ΔG, and ΔS are enthalpy change, free enthalpy change, and entropy change, respectively. R is the gas constant $8.314\ J\ mol^{-1}\ K^{-1}$, and T is the temperature. K represents the binding constant at the corresponding temperature. Results are shown in Table 1. The negative sign for ΔG means that the binding

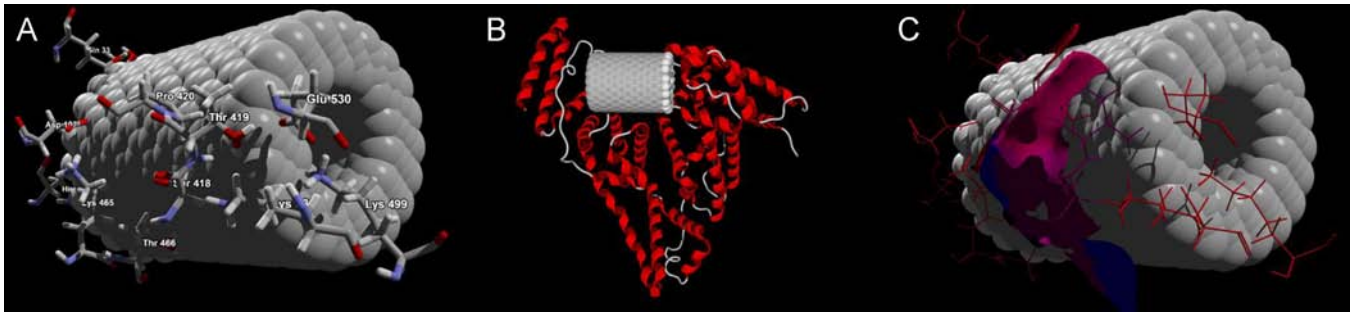

Fig. 3. Computational interaction models of BSA–MWCNTs: (A) the residues of BSA are represented using sticks and the MWCNTs are represented using the CPK model, (B) secondary structure view: BSA represented by solid ribbons and MWCNTs are represented using the CPK model, and (C) hydrophobicity view: binding pockets of protein are represented by hydrophobic interaction and MWCNTs are represented using the CPK model.

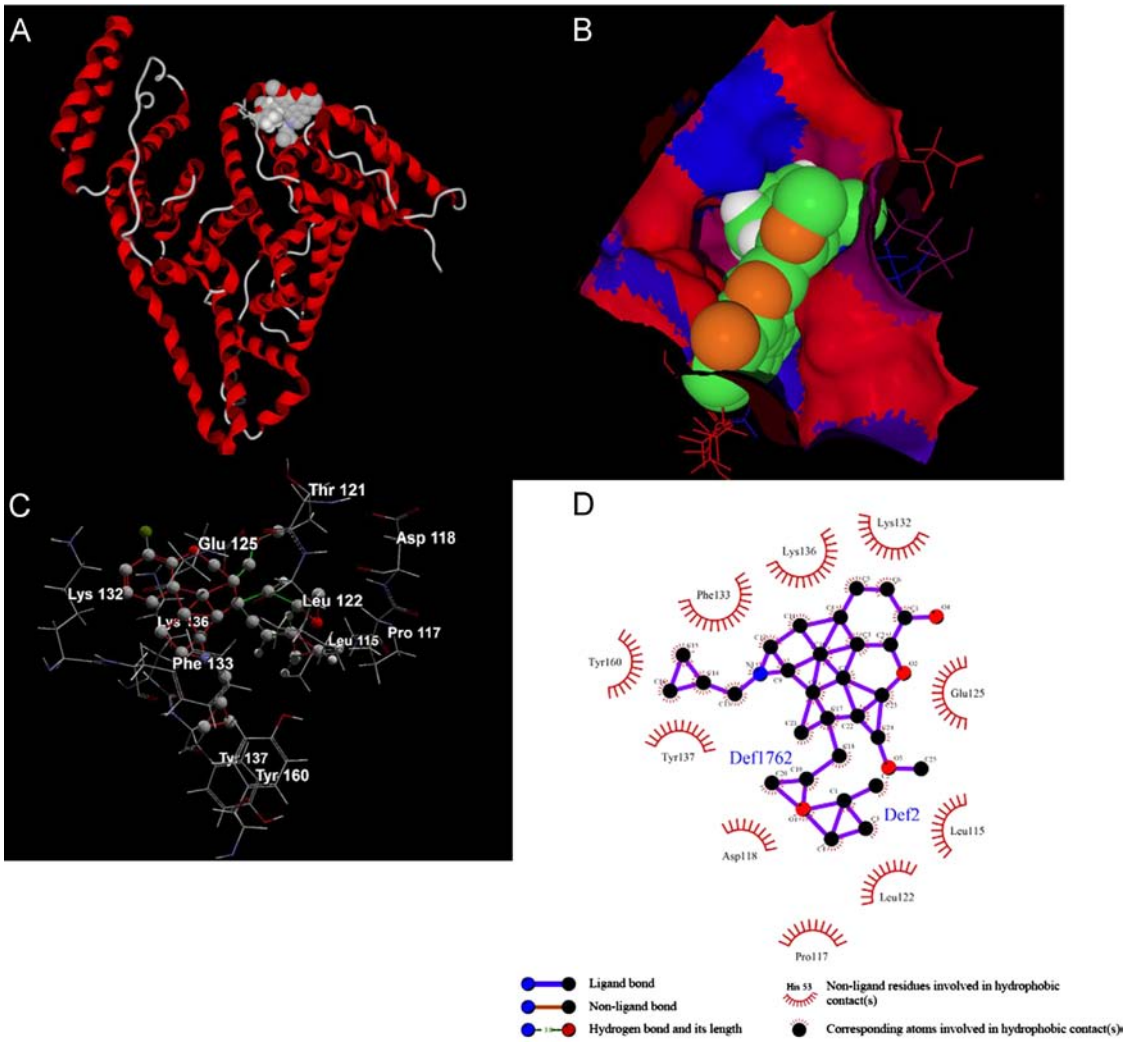

Fig. 4. Computer-generated models of BN bound to BSA: (A) secondary structure view: the BN is shown by CPK and BSA is represented by solid ribbons, (B) the residues of BSA are represented using sticks (thin) and the BN is represented using ball and stick, (C) the binding pocket of protein is represented by hydrophobic interaction and BN is shown as the CPK model, and (D) the output of LIGPLOT program.

process is spontaneous. The positive values of ΔS and ΔH reveal the predominance of hydrophobic interactions in the binding of MWCNTs with BSA.

The same procedure as previous one was used to study the interaction of BN with BSA (Fig. 5B) and the results are given in Table 1. The results showed that binding of BN with BSA is driven by hydrophobic interactions.

3.2.1.2. UV–vis absorption studies. UV–vis absorption measurement is a simple but efficacious method to explore structural changes and show complex formation. Therefore, in order to explore the structural change in BSA and to confirm the complex formation between MWCNTs and BSA, the UV–vis absorption measurements were carried out [31]. Hyperchromicity occurred in UV absorption spectra of BSA upon addition of MWCNTs (not shown) which confirmed the absorption of BSA on MWCNTs. The peak at 280.0 nm originates from the π–π^* transition of aromatic amino acid residues such as tryptophan and tyrosine [32]. Generally, the micro-environment surrounding amino acid residues are resolved by molecular conformation of the protein. Moreover, UV absorption spectra generate the corresponding change with alteration in the micro-environment. Therefore, changes in the spectral characteristics of BSA are used to judge the conformational changes. The intensity of UV absorption spectra of BSA increases noticeably. Moreover, a blue-shift emerges in maximum absorption wavelength (λ_{max}) from 280.0 nm to 277.0 nm, demonstrating the increase in hydrophobicity of amino acid residues. Changes in λ_{max} indicated the change in peptide strand of BSA molecules and hence the change in hydrophobicity. From these, we propose that the binding between MWCNTs and BSA molecules led to changes in protein conformation.

In order to explore the structural change in BSA and to confirm the complex formation between BN and BSA, the UV–vis absorption measurements were also made. The UV–vis absorption studies were carried out by keeping the BN concentration constant and increasing the concentration of BSA (Fig. 5C). It was evident that the intensity of UV absorption of BN changed with the addition of BSA concentration. BN exhibited a maximum absorption at 285.0 nm. The absorbance of BN at 285.0 nm increased regularly upon the addition of BSA. Moreover, the maximum peak position of BN–BSA was shifted (6.0 nm) towards lower wavelength region. The UV–vis absorption studies were also carried out by keeping the BSA concentration constant and increasing the concentration of BN (Fig. 5D). BSA has an absorption peak at 280.0 nm. This peak was found to be shifted to 5.0 nm towards higher wavelength in the presence of increased amounts of BN

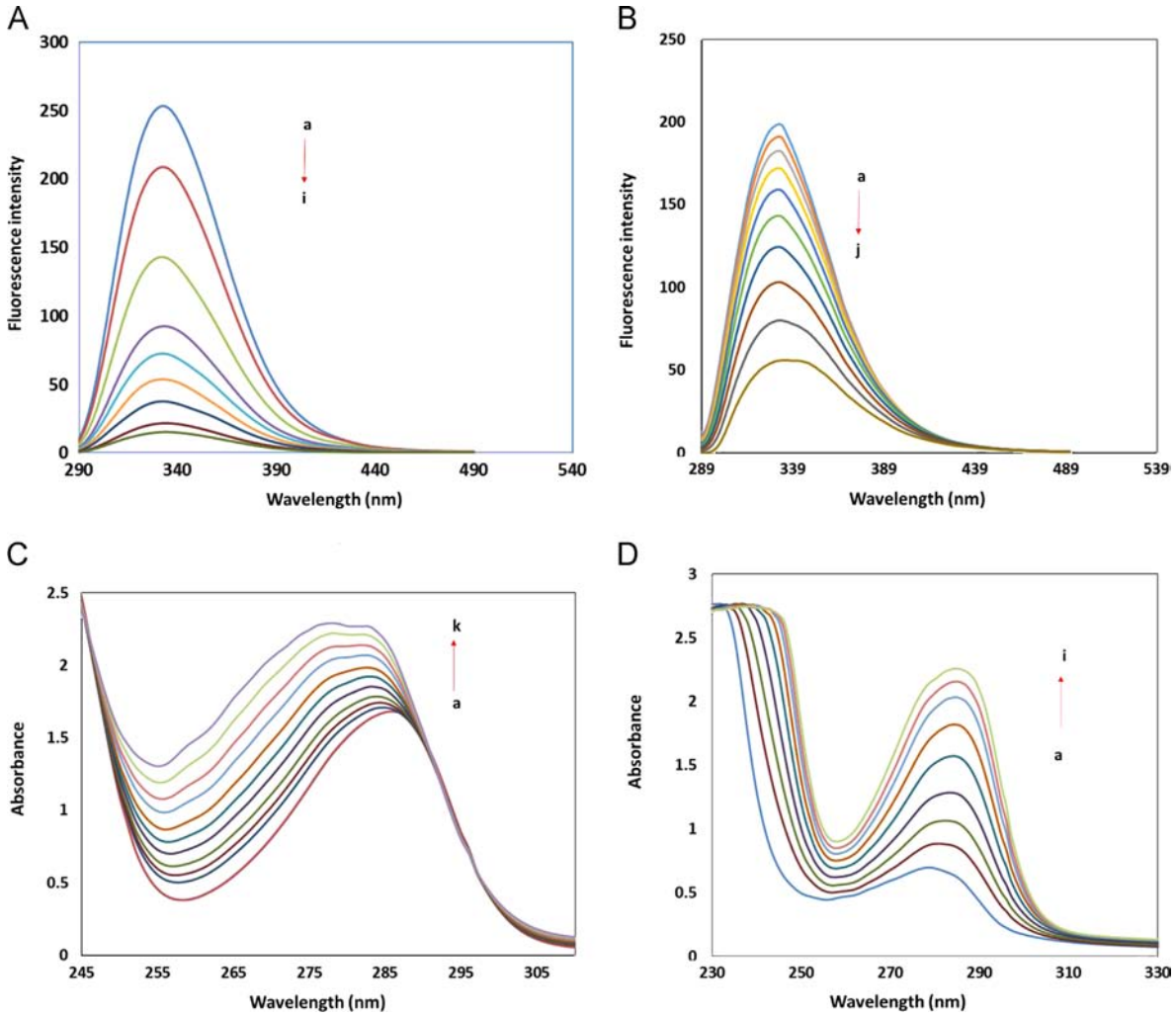

Fig. 5. (A) Fluorescence emission spectra of the BSA–MWCNTs system in PBS (0.067 M, pH 7.4) at 298.15 K: (a) free BSA (20.0 μM), and (b–i) BSA 20.0 μM with MWCNTs at 5.0, 10.0, 20.0, 30.0, 40.0, 50.0, 60.0, and 80.0 μM, (B) fluorescence emission spectra of the BSA–BN system in PBS (0.067 M, pH 7.4) at 298.15 K: (a) free BSA (15.0 μM), and (b–j) BSA 15.0 μM with BN at 2.0, 4.0, 5.0, 10.0, 20.0, 30.0, 40.0, 50.0, and 60.0 μM, (C) UV–vis absorption spectra of the BN–BSA system in PBS (0.067 M, pH 7.4): (a) free BN (1.0 μM), and (b–k) BN 1.0 μM with BSA at 0.1, 0.2, 0.3, 0.4, 0.5, 0.6, 0.7, 0.8, 0.9, and 1.0 μM, and (D) UV–vis absorption spectra of the BSA–BN system in PBS (0.067 M, pH 7.4): (a) free BSA (1.0 μM), and (b–i) BSA 0.5 μM with BN at 0.5, 1.0, 1.5, 2.0, 2.5, 3.0, 3.5, and 4.0 μM.

Table 1
Estimated thermodynamic parameters for BSA–MWCNTs and BSA–BN systems.

T (K)	10^{-4} K_a (M^{-1})	n	ΔH (kJ mol^{-1})	ΔS (J mol^{-1} K^{-1})	ΔG (kJ mol^{-1})
BSA–MWCNTs					
298.15	29	1.93	39.5	180.4	−14.28
304.15	36	1.99			−15.34
310.15	41	2.03			−16.45
BSA–BN					
298.15	3.8	1.86	35.3	185.2	−19.92
304.15	4.1	1.91			−21.03
310.15	4.3	1.98			−22.14

(Fig. 5D). From these results, we propose that the binding between BN and BSA led to changes in protein conformation.

3.2.2. Morphological studies of the composite electrodes

Fig. 6A and B shows the SEM images of MWCNTs/GCE and BSA/MWCNTs/GCE, respectively. The SEM image of MWCNTs/GCE (Fig. 6A) shows the MWCNTs twining around each other and attached to the GCE. It is clear that MWCNTs almost homogeneously distributed on the electrode surface by forming a thin layer. When BSA was immobilized on the electrode surface the clear MWCNTs image became dim and the protein adsorbed and aggregated onto the surface of the tubes (Fig. 6B); therefore, it demonstrated that MWCNTs were wrapped by BSA.

3.2.3. Optimization studies

In order to obtain satisfied assay result, some factors are investigated in detail. It was found that the amounts of MWCNTs and BSA deposited on the electrode surface, and incubation time with BN greatly affected the electrochemical response of the biosensor. To optimize the recorded signal, the performance of the biosensors fabricated with different concentrations of MWCNTs and BSA was studied under different incubation times with the same concentration of target BN (50.0 nM). The change of ΔR_{ct} ($\Delta R_{ct}=R^0_{ct}-R_{ct}$, R_{ct}: charge transfer resistance) was used to characterize the change of electrode surface. It was clearly observed that the ΔR_{ct} increased with the increase of amount of MWCNTs when the concentration of MWCNTs was 0.5 mg mL^{-1}. Hence, 0.5 mg mL^{-1} of MWCNTs was chosen as the optimized concentration for the next experiments. Next, the amount of BSA on MWCNTs/GCE surface and incubation time of BSA/MWCNTs/GCE with BN were checked. It was found that the ΔR_{ct} signals

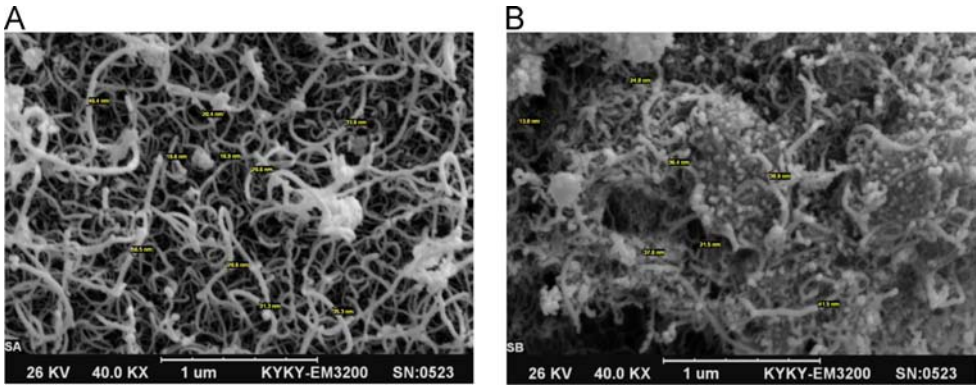

Fig. 6. SEM images of (A) MWCNTs/GCE, and (B) BSA/MWCNTs/GCE.

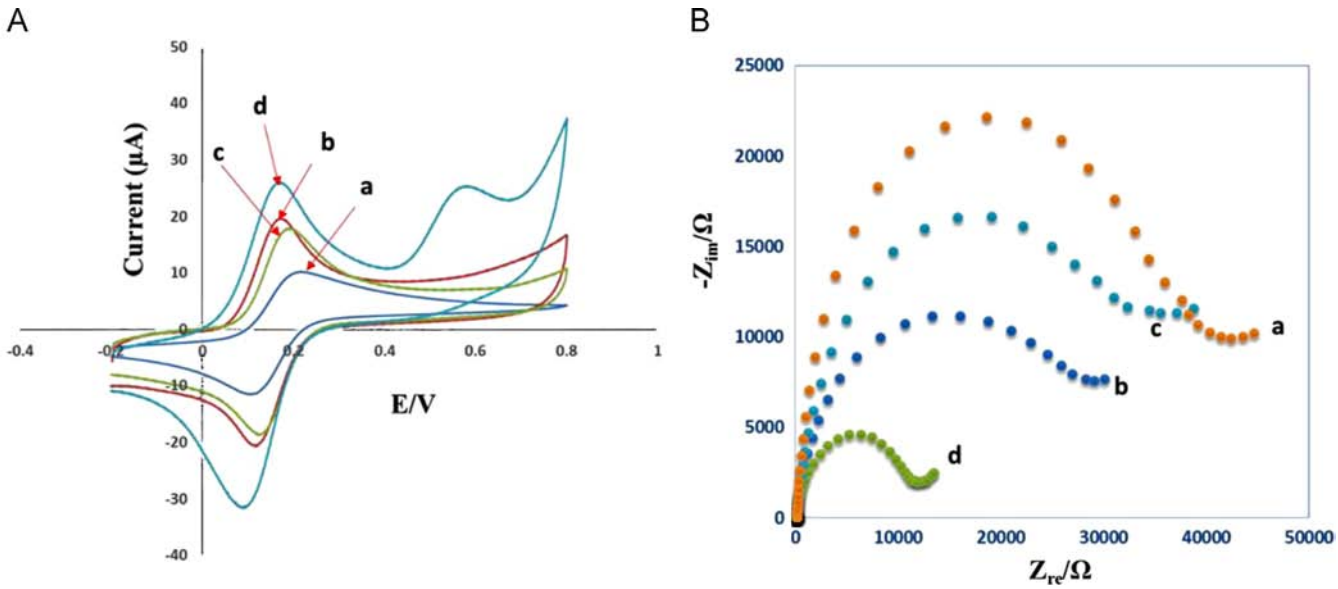

Fig. 7. (A) CVs and (B) EISs of 5.0 mM $[Fe(CN)_6]^{3-/4-}$ in PBS 0.067 M, pH 7.4 at a scan rate of 50.0 mV s^{-1} on (a) bare GCE, (b) MWCNTs/GCE, (c) BSA/MWCNTs/GCE, and (d) BSA/MWCNTs/GCE incubated with BN (50.0 nM) for 30.0 min.

increased rapidly with the decrease of BSA amount and increase of incubation time, when the concentration of BSA and incubation time were 0.35 mg mL^{-1} and 30.0 min, respectively. Thus, these optimized values were used in the standard procedures.

3.2.4. Electrochemical studies

The cyclic voltammograms (CVs) of 5.0 mM $[Fe(CN)_6]^{3-/4-}$ in PBS 0.067 M, pH 7.4 at a scan rate of 50.0 mV s^{-1} on bare GCE, MWCNTs/GCE, BSA/MWCNTs/GCE, and also BSA/MWCNTs/GCE incubated with BN (50.0 nM) for 30.0 min were investigated. A standard redox peak could be found for the bare GCE (Fig. 7A, curve a). The background currents and the redox peaks' currents of MWCNTs/GCE, and BSA/MWCNTs/GCE (Fig. 7A, curves b and c) were larger than those of bare GCE, which indicated that they have larger effective surface areas. After modification of the GCE with MWCNTs the peak current increased, and the ΔE_P decreased, showing the enhancement in the rate of electron transfer at the MWCNTs/GCE surface. After MWCNTs/GCE coated with BSA, it could be seen that the redox currents of the probe decreased, the peak potentials change a little, and no new peak is found in the same potential range. Thus, it is proposed that the presence of BSA inhibits the interfacial electron transfer to some extent due to the non-conductive properties of BSA which acted as an inert electron layer and hindered the electron transfer. On the other hand, when the BSA/MWCNTs/GCE was further incubated in BN solution, it could be seen that the redox currents and the ΔE_P increased and decreased (Fig. 7A, curve d), respectively. Thus, according to these observations and the new peak at 0.581 V, it is proposed that BN may form a positively charged electroactive complex with BSA which accelerates the electron transfer of the negatively charged redox probe due to the electrostatic attraction between the electrode surface and the redox couple ions carrying negative charge.

The enhanced peak current may be owed to the enlargement in the effective surface area. Therefore, to investigate this factor, the surface areas of the prepared electrodes were evaluated by the Randles–Sevcik equation (298.15 K), using the redox currents of the redox probe (i_p):

$$i_p = (2.687 \times 10^5) n^{3/2} \upsilon^{1/2} D^{1/2} A C \quad (4)$$

where D, the diffusion coefficient of the ferricyanide, was 6.3×10^{-6} cm^2 s^{-1}; n and C represent the transferring electron number and the concentration (mol dm^{-3}) of the ferricyanide; υ was the scan rate (V s^{-1}); and A was the surface area (cm^2).

The surface areas of the bare GCE, MWCNTs/GCE, BSA/MWCNTs/GCE, and BSA/MWCNTs/GCE incubated with BN (50.0 nM) for 30.0 min were calculated to be 0.17, 0.24, 0.22, and 0.32 cm^2, respectively.

The EIS can be used as an effective method for probing the features of interfacial electron-transfer resistance during the modification process. In the Nyquist diagram, the diameter of the semicircle reflects the R_{ct} of redox conversion of $[Fe(CN)_6]^{3-/4-}$ at the electrode surface. In this study, we focused on the R_{ct} between the solution and the electrode surface. The electron transfer process is caused by the presence of $[Fe(CN)_6]^{3-/4-}$ couple in the bulk solution. Any modification of the electrode surface strongly influences its electrochemistry, thus leads to a change in the R_{ct} value. Fig. 7B shows the EISs of 5.0 mM $[Fe(CN)_6]^{3-/4-}$ in PBS 0.067 M, pH 7.4 at bare GCE (curve a), MWCNTs/GCE (curve b), BSA/MWCNTs/GCE (curve c), and BSA/MWCNTs/GCE after treatment with BN (curve d). It can be seen that at the GCE, a semicircle with R_{ct} about 41.4 kΩ was obtained. However, the diameters of the semicircles were changed to 29.08 kΩ and 34.5 kΩ by modification of the GCE with MWCNTs, and BSA/MWCNTs, respectively, suggested that acceleration and deceleration for $[Fe(CN)_6]^{3-/4-}$ redox reaction occurred due to the presence of MWCNTs and BSA, respectively. A conceivable reason for the increase in the R_{ct} value during the modification of MWCNTs/GCE with BSA is that BSA acts as an inert electron layer which hinders the interfacial electron transfer to some extent. On the other hand, by treating the BSA/MWCNTs/GCE with BN, the interfacial electron resistance decreased dramatically (10.2 kΩ) which indicates a fast charge transfer of the redox probe coinciding with the CV results. Thus, BN addition would result in the activation of the BSA/MWCNTs/GCE surface by forming a positively charged electroactive complex with BSA which attracts the negatively charged redox probe and accelerates the interfacial electron transfer and leads to obvious Faradaic impedance change.

3.2.5. Analytical application

3.2.5.1. BN determination. Under the optimized conditions, the relationship between $\Delta R/R^0_{ct}$ values and the concentrations of synthetic BN samples was studied (Fig. 8). As shown in the inset of Fig. 8, there is a linear relationship between $\Delta R/R^0_{ct}$ and the concentration of BN over a concentration range from 5.0 nM to 72.0 nM (R^2 0.992). The linear response obtained with the biosensor indicated that the sensor could be possibly used in the analysis of real samples. The limit of detection (LOD) of this method was calculated by following IUPAC recommendations ($3S_b/b$, where S_b is the standard deviation ($n=8$) of the blanks, and b is the slope value of the respective calibration graph) at a concentration level of 1.5 nM. Moreover, the sensitivity for BN determination calculated from the slope of the respective calibration graph was 0.01 KΩ nM^{-1}, indicating the high sensitivity of the proposed sensing system. This work is the first report on the BN biosensor; therefore, we could not make a comparison between its results with those reported in literatures but, in next sections we will make a comparison between the results obtained by the proposed biosensor in determining BN in real samples with those of the HPLC-UV method.

3.2.5.2. Stability, repeatability, and reproducibility. The stability of BSA/MWCNTs/GCE was investigated by measuring a fresh solution of 20.0 nM BN in PBS (0.067 M, pH 7.4) containing 5.0 mM $[Fe(CN)_6]^{3-/4-}$. Ten days later the response of the biosensor retained 94.3% of its initial value. After 1 month of testing, the biosensor response decreased about 9.5%. As well, the duration time of immersing biosensor in the cell solution affected the stability behavior of measurements. The biosensor gave good stability during the impedimetric time scale while its functions were not good enough when it continued in contact with aqueous surrounding electrolyte for more than 6.0 h. Therefore, it is recommended to remove the working electrode from the electrochemical cell solution during the breaks between measurements. The repeatability of the proposed biosensor was tested for ten times within the same day giving satisfied relative standard deviation (RSD) of 3.1%. The reproducibility of the BSA/MWCNTs/GCE was examined by recording the EIS responses of six individual electrodes in 5.0 mM $[Fe(CN)_6]^{3-/4-}$ in PBS (0.067 M, pH 7.4) containing 20.0 nM BN and the RSD was obtained as 4.2%. The above results indicated the good stability, repeatability, and reproducibility of the proposed biosensor.

3.2.5.3. Interference study. To evaluate the selectivity of the proposed biosensor, some possible interfering species such as thiourea, dopamine, urea, uric acid, sucrose, fructose, glucose, and ascorbic acid, which may be present in real samples, were tested in 5.0 mM $[Fe(CN)_6]^{3-/4-}$ in PBS (0.067 M, pH 7.4), with a mixed BN concentration of 20.0 nM. After the experiment, we concluded that 100.0-fold thiourea, dopamine, urea, and uric acid, 50.0-fold sucrose, fructose, and 20.0-fold glucose, and ascorbic acid did not show remarkable interference to BN determination.

3.2.5.4. Determination of BN in real samples. To assess the BSA/MWCNTs/GCE's ability to determine BN in real samples, we tested its ability to detect BN in urine samples in both healthy and addict volunteers. Results are summarized in Table 2. The good recoveries suggested that impedimetric determination of BN using the proposed biosensor was effective and sensitive. The accuracy of

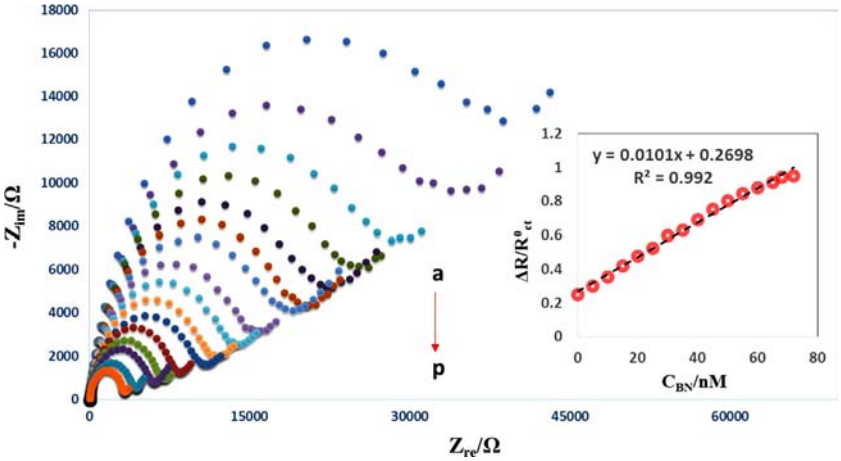

Fig. 8. (A) EIS curves of the BSA/MWCNTs/GCE in a $[Fe(CN)_6]^{4-/3-}$ solution (0.067 M, pH 7.4) corresponding to different concentrations of BN. (a) 0.0, (b) 5.0 nM, (c) 10.0 nM, (d) 15.0 nM, (e) 20.0 nM, (f) 25.0 nM, (g) 30.0 nM, (h) 35.0 nM, (i) 40.0 nM, (j) 45.0 nM, (k) 50.0 nM, (l) 55.0 nM, (m) 60.0 nm, (n) 65.0 nM, (o) 68.0 nM, and (p) 72.0 nM. (Inset) The corresponding calibration plot of $\Delta R/R^0_{ct}$ versus different concentrations of BN.

Table 2
Determination of BN in urine samples ($n=4$).

Samples	Added (nM)	Found (nM)	Recovery (%)	HPLC-UV
Urine[h]	10.0	10.2 ± 0.1	102.0	10.1 ± 0.1
	7.0	7.1 ± 0.2	101.4	7.0 ± 0.1
	–	< LOD	–	< LOD
	8.0	7.9 ± 0.1	98.7	8.0 ± 0.1
Urine[a]	–	20.0 ± 1.2	–	20.3 ± 0.5
	5.0	25.3 ± 0.3	105.7	25.1 ± 0.2
	15.0	34.6 ± 0.7	97.3	35.0 ± 0.2
	35.0	56.0 ± 0.5	102.8	55.2 ± 0.5

[h] Healthy volunteer.
[a] Addict volunteer.

the results of the proposed biosensor was compared with HPLC-UV results. The chromatographic separation was performed on a Poroshell 120 EC-C18 analytical column (100 mm × 4.6 mm × 2.7 μm) (Agilent Technologies, Wilmington, DE, USA).The mobile phase consisted of 60.0% buffer containing 10.0 mM NaH_2PO_4, 0.7 mM sodium dodecyl sulfate and 40.0% acetonitrile. The pH of the aqueous buffer in the mobile phase was adjusted to 7.4. The flow-rate of the mobile phase was adjusted to 1.0 mL min^{-1} and the detection was performed at the wavelength of 285.0 nm. The results presented in Table 2 confirmed that the results obtained by the proposed biosensor were satisfactory and comparable to those obtained by applying the reference HPLC-UV method. Compared with the HPLC-UV method, the proposed biosensor is simple, easily implemented, and has low-cost and fast response. Thus, accurate and successful determination of BN in biological fluids as demonstrated here may allow one to propose the present biosensor as a promissory, cheap and accessible alternative for the clinical analysis of BN.

4. Conclusions

In summary, an ultrasensitive impedimetric BN biosensor based on immobilization of BSA/MWCNTs nanobiocomposite onto GCE was presented. The proposed biosensor exhibited stable, regenerable, and sensitive functions for BN determination. The characterizations performed by cyclic voltammetry, and electrochemical impedance spectroscopy suggested that the incubation of BSA/MWCNTs/GCE with BN significantly increases the electrode surface area and leads to obvious Faradaic impedance changes. Besides providing a better understanding of the physical and chemical parameters involved in the development of BSA/MWCNTs nanobiocomposite, the present manuscript provides evidence of the advantages related to the use of computational techniques, in particular in regard to the rational elaboration of biosensors. The principles used in this study could potentially be used to construct new biosensors in clinical settings for biological fluids.

Acknowledgments

The authors gratefully acknowledge the financial supports of this project by the Razi University Research Council, UNL, CONICET and ANPCyT.

References

[1] R.C. Heel, R.N. Brogden, T.M. Speight, G.S. Avery, Drugs 17 (1979) 81–110.
[2] G.F. Koob, N.D. Volkow, Neuropsychopharmacol. Rev. 35 (2010) 217–238.
[3] P.J. Hoskin, G.W. Hanks, Drugs 41 (1991) 326–344.
[4] J. Strang, Lancet 2 (1985) 725–726.
[5] L. Debrabandere, M. Van Boven, L. Laruella, P. Daenens, Anal. Chim. Acta 275 (1993) 295–303.
[6] M.A. García-Fernández, M.T. Fernández-Abedul, A. Costa-García, Electroanalysis 12 (2000) 483–489.
[7] P. Nikolaou, I. Papoutsis, S. Athanaselis, C. Pistos, A. Dona, C. Spiliopoulou, Biomed. Chromatogr. 26 (2012) 358–362.
[8] F. Vincent, J. Bessard, J. Vacheron, M. Mallaret, G. Bessard, J. Anal. Toxicol. 23 (1999) 270–279.
[9] D.E. Moody, J.D. Laycock, A.C. Spanbauer, D.J. Crouch, R.L. Foltz, J.L. Josephs, L. Amass, W.K. Bickel, J. Anal. Toxicol. 21 (1997) 406–414.
[10] I.I. Papoutsis, P.D. Nikolaou, S.A. Athanaselis, C.M. Pistos, C.A. Spiliopoulou, C.P. Maravelias, J. Pharm. Biomed. Anal. 54 (2011) 588–591.
[11] H. Hoja, P. Marquet, B. Verneuil, H. Lotfi, J.L. Dupuy, G. Lachâtre, J. Anal. Toxicol. 21 (1997) 160–165.
[12] D.E. Moody, M.H. Slawson, E.C. Strain, J.D. Laycock, A.C. Spanbauer, R.L. Foltz, Anal. Biochem. 306 (2002) 31–39.
[13] S. Hegstad, H.Z. Khiabani, E.L. Qiestad, T. Berg, A.S. Christophersen, J. Anal. Toxicol. 31 (2007) 214–219.
[14] A. Ceccato, R. Klinkenberg, P. Hubert, B. Streel, J. Pharm. Biomed. Anal. 32 (2003) 619–631.
[15] A. Polettini, M.A. Huestis, J. Chromatogr. Biomed. Sci. Appl. 754 (2001) 447–459.
[16] M. Scislowski, W. Piekoszewski, A. Kamenczak, E. Florek, J. Anal. Toxicol. 29 (2005) 249–253.
[17] A. Tracqui, P. Kintz, P. Mangin, J. Forensic Sci. 42 (1997) 111–114.
[18] A.A. Ensafi, E. Khoddami, B. Rezaei, H. Karimi-Maleh, Colloids Surf. B 81 (2010) 42–49.
[19] A.A. Ensafi, H. Karimi-Maleh, J. Electroanal. Chem. 640 (2010) 75–83.
[20] A.A. Ensafi, S. Dadkhah, B. Rezaei, J. Serbian Chem. Soc. 75 (2010) 1685–1699.
[21] A.A. Ensafi, M. Taei, T. Khayamian, A. Arabzadeh, Sens. Actuators B 147 (2010) 213–221.
[22] A.A. Ensafi, S.Z. Mirahmadi Zare, B. Rezaei, M. Taei, Sens. Actuators B 150 (2010) 321–329.
[23] G.C. Zhao, L. Zhang, X.W. Wei, Z.S. Yang, Electrochem. Commun. 5 (2003) 825–829.
[24] L.Y. Zhao, H.Y. Liu, N.F. Hu, Anal. Bioanal. Chem. 384 (2006) 414–422.
[25] X. Yu, D. Chattopadhyay, I. Galeska, F. Papadimitrakopoulos, J.F. Rusling, Electrochem. Commun. 5 (2003) 408–411.
[26] A.A. Ensafi, E. Khoddami, B. Rezaei, Talanta 116 (2013) 1113–1120.
[27] A.C. Wallace, R.A. Laskowski, J.M. Thornton, Protein Eng. 8 (1995) 127–134.
[28] J.R. Lakowicz, Principles of Fluorescence Spectroscopy, 3rd ed., Springer Press, New York, 2006.
[29] Y.-J. Hu, Y. Liu, X.-H. Xiao, Biomacromolecules 10 (2009) 517–521.
[30] P.D. Ross, S. Subramanian, Biochemistry 20 (1981) 3096–3102.
[31] S. Bi, D. Song, Y. Tian, X. Zhou, Z. Liu, H. Zhang, Spectrochim. Acta 61 (2005) 629–636.
[32] A.N. Glazer, E. Smitth, J. Biochem. 236 (1961) 2942–2947.